Article

pH-Dependent Conformations of an Antimicrobial Spider Venom Peptide, Cupiennin 1a, from Unbiased HREMD Simulations

Jokent T. Gaza, Jarold John C. Leyson, Gardee T. Peña, and Ricky B. Nellas*

Read Online

ACCESS | Metrics & More | Article Recommendations

ABSTRACT: Cupiennin 1a is an antimicrobial peptide found in the venom of the spider *Cupiennius salei*. A highly cationic peptide, its cell lysis activity has been found to vary between neutral and charged membranes. In this study, Hamiltonian replica-exchange molecular dynamics (HREMD) was used to determine the conformational ensemble of the peptide in both charged (pH 3) and neutral (pH 11) states. The obtained free energy landscapes demonstrated the conformational diversity of the neutral peptide. At high pH, the peptide was found to adopt helix−hinge−helix and disordered structures. At pH 3, the peptide is structured with a high propensity toward α-helices. The presence of these α-helices seems to assist the peptide in recognizing membrane surfaces. These results highlight the importance of the charged residues in the stabilization of the peptide

structure and the subsequent effects of pH on the peptide's conformational diversity and membrane activity. These findings may provide insights into the antimicrobial activity of Cupiennin 1a and other amphipathic linear peptides toward different cell membranes.
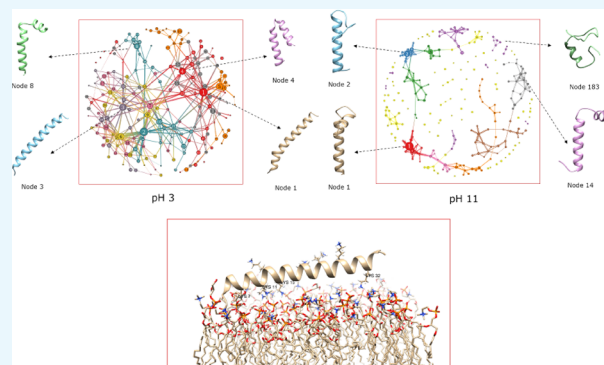
INTRODUCTION

Spider venom contains a cocktail of cytotoxic and neurotoxic compounds capable of paralyzing prey and facilitating external digestion. Venom components may be classified as (a) low-molecular-weight compounds that include salts, amines, and acylpolyamines; (b) linear and disulfide-linked peptides; and (c) enzymes and large proteins.[1−4] Neurotoxic components include acylpolyamines, cysteine-rich peptides, and large proteins that modulate the ion channels causing the nervous system to shut down.[5,6] The cytotoxic components of the venom, such as the amphipathic linear peptides, damage cells and tissues during envenomation to allow further penetration of toxins.[7] Enzymes in the venom such as lipases and proteases aid during external digestion of the prey prior to feeding.[7] These toxicological properties have attracted various studies on medical and agricultural applications of the venom components.[8]

An interesting function of the amphipathic linear peptides aside from neurotoxicity is their antimicrobial activity.[9−14] Antimicrobial peptides (AMPs), or host defense peptides (HDPs), in the venom play a role in preventing infection against microbial agents that accompany decomposition during external digestion.[11,15]

Several AMPs that showed promising activities have already been isolated and identified. Latarcins are short amphipathic antimicrobial peptides found in the venom of *Lachesana tarabaevi*.[16] Oxypinins from the Oxyopidae family are the

largest linear cationic amphipathic peptides to be identified from spider venom. Peptides isolated from the crude venom of *Oxyopes kitabensis* exhibit antimicrobial, hemolytic, and insecticidal activities.[11] Several peptides, like gomesins, have been isolated and identified from the crude venom of *Lasiodora* sp. of the Theraposidae family that also showed antibacterial and antifungal activities.[1,17] Cupiennin 1a is a basic antimicrobial peptide from the *Cupiennius salei* of the Trechaleidae family. With an estimated pI of 11.3, the peptide is highly cationic at neutral and low pH conditions due to its eight charged lysine residues.[18] The peptide has also been shown to adopt α-helical structures from coil conformations upon interactions with the lipid membranes.[18,19] Its mechanism of cell lysis has been found to vary between neutral and charged membranes.[20]

Circular dichroism studies have shown that Cupiennin 1a is unstructured in aqueous solutions.[18,20,21] Its mechanism of action, however, is linked with its tendency to form helical structures (Figure 1). In a membrane mimicking solvent of
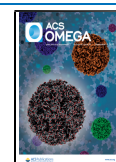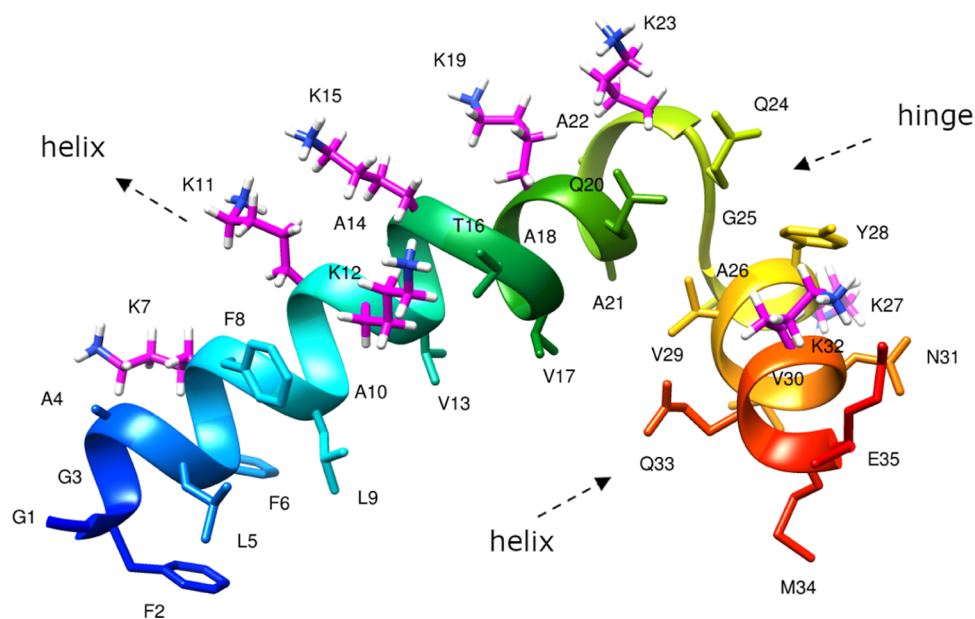
Figure 1. Helix−hinge−helix conformation of Cupiennin 1a obtained from the Hamiltonian replica-exchange molecular dynamics (HREMD) simulations. The eight lysine residues are represented by the purple stick model. Nonlysine hydrogen atoms were omitted for clarity purposes. The structure was visualized using UCSF Chimera software. The initial structure for the HREMD simulations was obtained from the protein data bank (ID 2K38). Sequence: GFGAL FKFLA KKVAK TVAKQ AAKQG AKYVV NKQME.
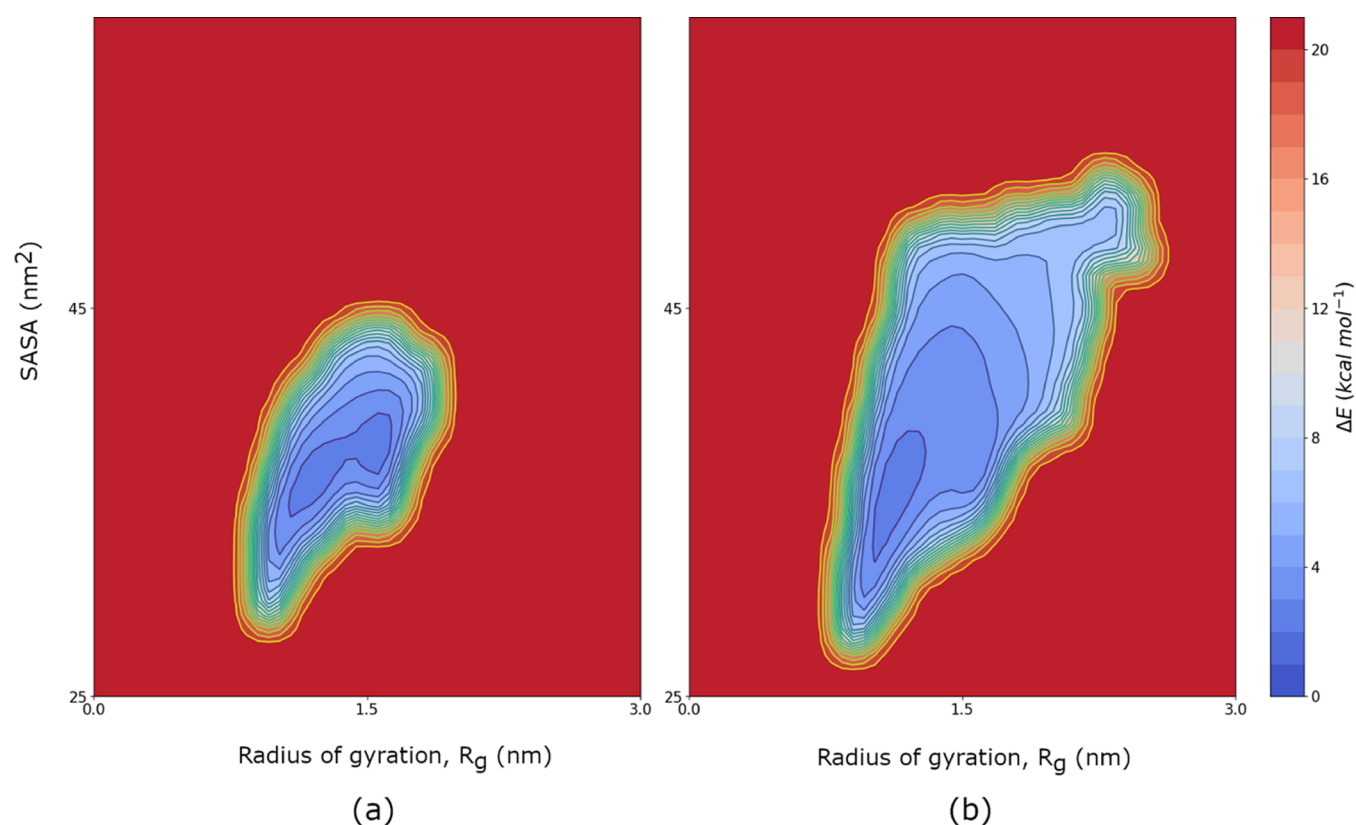

Figure 2. Free energy landscape of the two protein systems ((a) pH 3; (b) pH 11) as sampled by the HREMD simulation. The contours represent the estimated energy for each possible SASA (solvent-accessible surface area) and R_g (radius of gyration) pair. The difference in landscape sizes demonstrates the flexibility of the peptide at pH 11.

(1:1 v/v) trifluoroethanol and water (TFE/H_2O), the amphiphilic peptide forms a helix−hinge−helix structure that allows efficient entry of the peptide into the membranes.[20] The positively charged C-terminal seems to interact with the negatively charged surface of the membrane, while the amphipathic helix in the N-terminal inserts itself in the acyl region of the phospholipid bilayer.[18] These scenarios are facilitated by a disordered region, the hinge, by allowing the two regions to move independently of each other.[20]
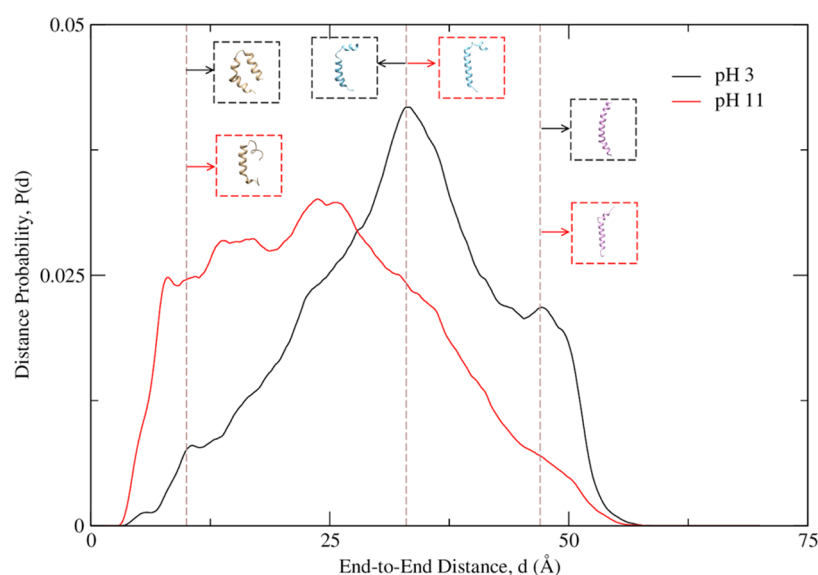
Figure 3. End-to-end distance values reported as probability distributions. The distances were calculated as the degree of separation between the α-carbons of the terminal residues 1 and 35. The calculation was done for all sampled conformations. The dashed brown lines correspond to distance values of 10, 33, and 48 Å. For each line, corresponding representative structures for both pH values were embedded. The dashed black boxes are for the pH 3 system, while the dashed red boxes are for pH 11.

Similar helix−hinge−helix conformations have also been observed in other antimicrobial peptides.[22−27] Melittin, for example, is a membrane-active amphiphilic peptide found in the venom of honey bees.[28,29] This pore-forming peptide displays potent antimicrobial properties on various Gram-positive and Gram-negative bacteria and also fast-developing mycobacteria.[30,31] In a lipid environment, melittin adopts a helix−hinge−helix structure.[32] The helical structure at the C-terminus aids in the recognition of lipopolysaccharides in the outer membrane of Gram-negative bacteria, while the hinge region seems to dictate the peptide's hemolytic activity.[33,34]

Highly active synthetic analogues of melittin and other naturally occurring AMPs have been designed for drug development purposes.[35,36] Among these are the MSI-78 and MSI-594 peptides.[37,38] MSI-78 is an analogue of magainin 2, a naturally occurring AMP found in the skin of *Xenopus laevis* frogs,[39,40] while MSI-594 is an analogue designed as a hybrid of MSI-78 and melittin.[41,42] Similar to their natural counterparts, the two analogues also seem to adopt helical conformations in a membrane mimicking environment.[42−44] Furthermore, MSI-78 forms stable dimers in DPC micelles, while MSI-594 prefers a monomeric conformation.[42]

In this study, an enhanced sampling method, Hamiltonian replica-exchange molecular dynamics (HREMD), was employed to probe the conformational space of Cupiennin 1a.[45−47] HREMD was implemented as recent studies placed emphasis on the use of enhanced sampling methods to generate structures of flexible peptides. Unbiased HREMD simulations were shown to produce an ensemble of structures that match the results of neutron and X-ray scattering and NMR experiments.[48,49]

The MD simulations were carried out at pH 3 and pH 11. These two pH conditions correspond to the peptide's charged and neutral states, respectively. Afterward, select structures have undergone structure−activity relationship studies through membrane-peptide MD simulations. Our study highlights the pH-dependent formation of α-helical structures in Cupiennin 1a and the peptide's conformational diversity in the neutral

state. Furthermore, our membrane-peptide simulations showed the importance of the charged lysine residues in the peptide's ability to recognize charged membrane surfaces.

RESULTS AND DISCUSSION

Different Conformational Landscapes. Flexible peptides are characterized by various structures in their conformational ensembles. This translates to a wide conformational space with numerous minima, each signifying a possible conformation for the peptide. Here, an enhanced sampling method was used to perform a thorough exploration of Cupiennin 1a's conformational space.

The free energy landscapes presented in Figure 2 represent the conformational space of the peptide at pH 3 and pH 11. The contours correspond to the probability of each solvent-accessible surface area (SASA) and radius of gyration (R_g) pair as dictated by the HREMD simulations. These two biophysical values provide insight into the general structure of the peptide. SASA quantifies sites that are buried or exposed from the solvent, while R_g describes the protein's size.

The difference in landscape sizes suggests that the neutral peptide is more unstructured compared to the charged peptide. It seemed to sample energetically less favored states with high SASA and R_g values, a characteristic indicative of a disordered structure (Figure 2b). The charged peptide, on the other hand, is restricted to highly funneled minima populated by low SASA−R_g pairs (Figure 2a). These two observations suggest that the charged peptide is highly structured.

Ordered and Disordered Peptides. The free energy landscapes provided a general view of the structures sampled by the HREMD simulations. To determine specific features of these structures, biophysical analyses were performed on the calculated conformations (Figure 3). The end-to-end distance values were computed to obtain insights into the peptide's topology. For the pH 3 system, the probability distribution graph is characterized by peaks at high end-to-end distances. The pH 11 system, on the other hand, has a flattened curve that spans from low to high distance values. Given that the
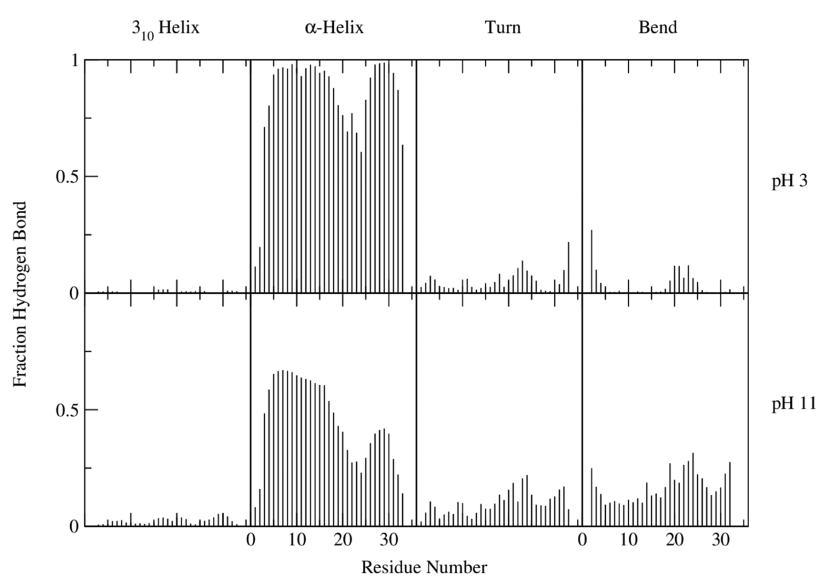
Figure 4. Secondary structures of each residue as obtained using the DSSP method. Calculations were done for all sampled conformations.
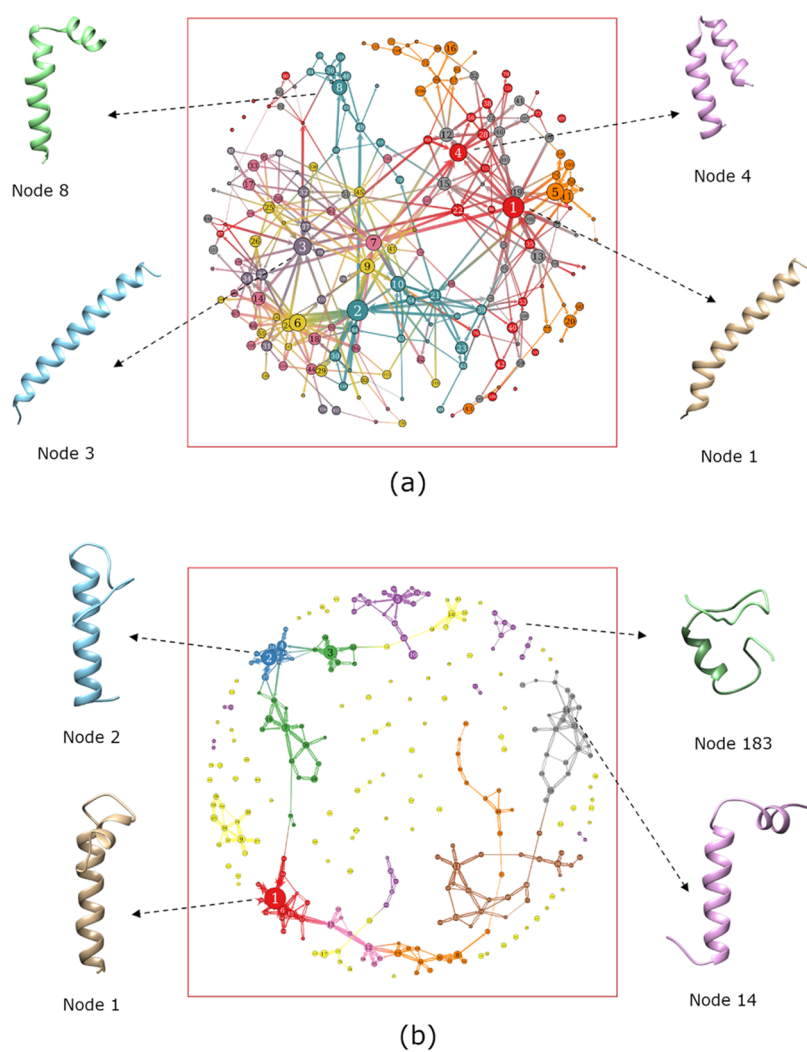

Figure 5. Network of conformations in the (a) pH 3 and (b) pH 11 systems and the corresponding representative structures of each major node. Node 183 was included to represent the disordered structure of the neutral peptide. The structure for each node of the conformational cluster transition network (CCTN) was determined using cpptraj and visualized through Python's graph-tool.
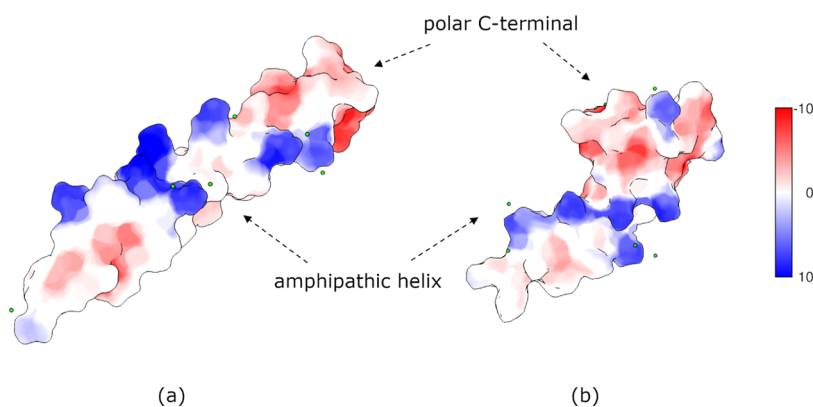
Figure 6. Coulombic surfaces of (a) full helical and (b) helix−hinge−helix structures. The color of the surfaces indicates the magnitude of the electrostatic potentials—red is negative (set at -10 kcal/mol), white is neutral, and blue is positive (10 kcal/mol). Chloride ions are represented by green circles. The interaction between the charged lysine residues and the negatively charged ions seems to stabilize the helices in both conformations. The structures were visualized using UCSF Chimera.

simulations started from an ordered helix−hinge−helix structure, the flat curve suggests that these helices were broken or became more coil-like for the neutral peptide.

To verify the results for the biophysical analyses, the peptide's propensity for secondary structures was quantified (Figure 4). The glaring difference between the α-helix values of the two systems indicates that the charged peptide prefers a more ordered helical structure than its neutral counterpart. The neutral peptide seems to sample-broken helix conformations as suggested by its higher turn and bend values. These observations are supported by the end-to-end distance values. Formation of broken helices allows interactions between the peptide's terminals. Integrating these results with the calculated free energy landscapes demonstrates the unstructured nature of the pH 11 system. Instead of a homogeneous ensemble consisting of compact and ordered structures, the ensemble sampled by the HREMD simulation for the neutral peptide is rather composed of conformations with variable size, shape, and structure.

To see how these structures might have correlated to each other, network analysis on the conformations was performed (Figure 5). Here, a cluster analysis was carried out on the sampled conformations. The clusters are portrayed by nodes, while the edges signify possible transitions between structures. The variable size of the node depends on the number of conformations represented by the cluster. For the pH 3 system, highly connected subnetworks were obtained (Figure 5a). Each major node in the network is connected to other multiple major nodes. The most visited cluster (Node 1), for instance, is connected to Nodes 2, 3, and 4 through multiple pathways. Visualization of these clusters shows that the most visited conformations are composed of full helical and helix−hinge−helix structures. These observations are supported by the obtained conformational landscapes and end-to-end results.

The network of conformations for pH 11, on the other hand, shows clear pathways between connected major nodes. In these connected regions, the nodes correspond to helix−hinge−helix structures with different C-terminal positions, as dictated by the hinge region. The edges represent the correlation between structures with seemingly independent helix regions. Another feature of the network is the independent nodes scattered throughout Figure 5b. We surmise that these nodes represent the disordered structures proposed by the biophysical results. The absence of edges

suggests that these are highly variable structures that are not related to other ordered or disordered structures. Visualization of these nodes showed a coil-like structure for the peptide. These mixes of structures, along with the biophysical results, reveal the disordered nature of the neutral peptide.

Structure−Activity Relationship. The cytolytic activity of Cupiennin 1a toward charged membranes has been linked with its amphipathic N-terminal and polar C-terminal.[18,50] The latter aids in the identification of cell membrane surfaces through electrostatic interactions, while the former permeabilizes membranes through toroidal pores.[19] In this scenario, Cupiennin 1a likely adopts a helix−hinge−helix structure, as found in previous NMR studies.[20] Likewise, experimental circular dichroism (CD) results showed that the peptide favors coil-like conformations in vesicle-less systems.[19]

In this study, however, the charged peptide in the vesicle-less solution primarily adopts the full helical or helix−hinge−helix structure. To explain the discrepancy between experimental and computational results, the Coloumbic surfaces of both structures were visualized (Figure 6). The propensity of charged Cupiennin 1a toward α-helices is induced by the negatively charged polar heads of lipids. Here, we surmise that the chloride ions in our system have the same function as these lipids. The excess chloride ions added to neutralize the system seem to interact with the protonated lysine residues of the peptide. This was observed in both full helical and helix−hinge−helix structures. For the neutral peptide, however, such a phenomenon was absent or minimal. For this system, there are equal numbers of potassium and chloride ions due to the neutral charge of the peptide. Furthermore, the amphipathic nature of the helices has been lost because of the deprotonation of lysine residues. This may have allowed destabilization of the helices and, consequently, facilitated the dynamic behavior of the neutral peptide.

We suspect the peptide structure at pH 11 to be similar to its inactive form, and the helical state at pH 3 to be the active form. To initiate its cytolytic activity, Cupiennin 1a has to recognize the negatively charged membranes. This then triggers a membrane-facilitated cascade of conformational changes for the peptide to adopt a helical form. In the absence of membranes, the peptide is likely in an equilibrium between ordered and disordered structures, similar to the results of the HREMD simulations for the pH 11 system. To verify this statement, molecular dynamics simulations of four protein-
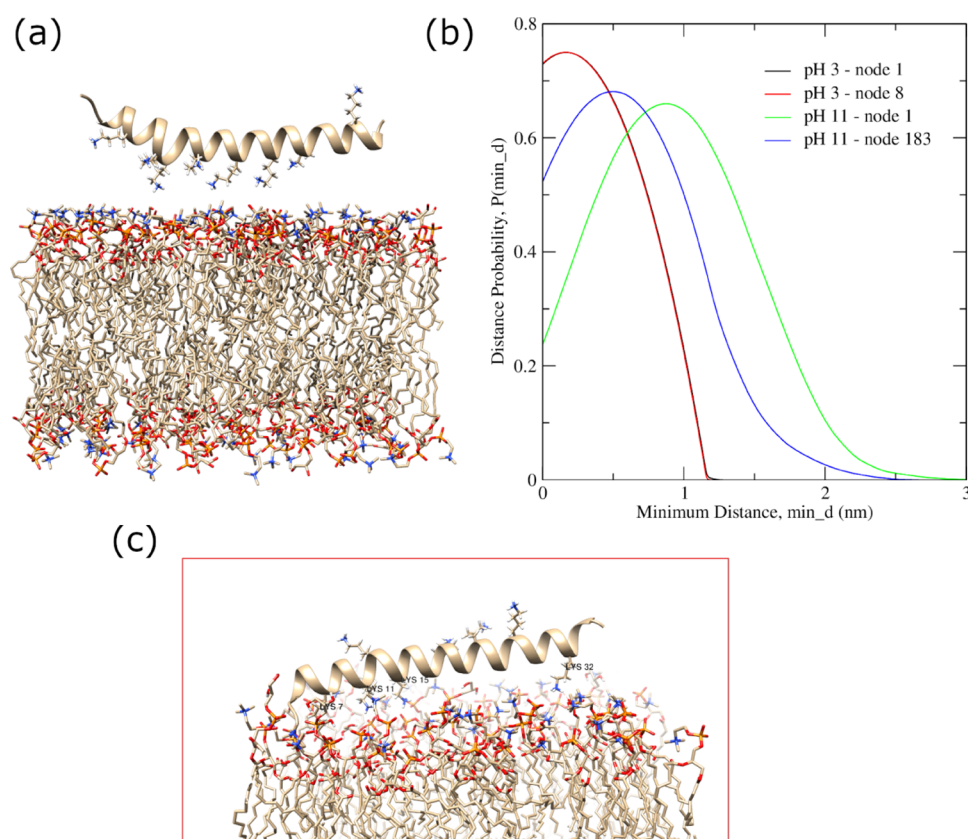
Figure 7. (a) Initial structure of the protein-membrane system for the full helical peptide at pH 3. Ions and water molecules were removed for clarity purposes. (b) Minimum distance values between lysine residues and membrane. The distance values were calculated between the nearest lysine residue and the membrane atom. (c) Last conformation from the MD simulation. Hydrogen bonds (dashed red line) were seen between the phosphate heads of the lipids and lysine residues 7 and 32.

membrane systems were performed (Figure 7a). The peptides in the four systems (two for each pH value) were obtained from the network analysis. The peptides were placed outside a 3:1 membrane mixture of DMPC and DMPG lipids with the lysine residues orientated toward the phospholipid heads, similar to a previous study on AMP PGLa.[51,52] The simulations were run for 30 ns and analyzed for possible interactions between the membrane surface and the peptides. To quantify this interaction, the minimum distance values between the lysine residues and the membrane were calculated.

Peptides under the pH 3 condition were found to have minimum distance peaks at around 2 Å (Figure 7b). This signifies that, for most of the simulations, the pH systems favor interactions between the charged lysine residues and the membrane surface (Figure 7c). The pH 11 systems, on the other hand, indicate that the neutral peptides have minimal interactions with the charged phosphate heads of the membrane. This observation coincides with the established activity of Cupiennin 1a toward charged membrane surfaces[20] and further highlights the importance of the lysine residues in the peptide's antimicrobial activity.

■ CONCLUSIONS

Amphiphilic linear peptides isolated from spider venom have been shown to have antimicrobial activity against different cell membranes. Cupiennin 1a, for instance, was found to have different cell lysis activity toward neutral and charged membranes. Here, HREMD simulations were performed to explore the conformational space of Cupiennin 1a at pH 3 and pH 11. Construction of free energy landscapes showed a heterogeneous ensemble of structures for the neutral peptide and highly helical structures for the charged system. Analyses of these structures revealed the disordered nature of the peptide at high pH levels.

The subsequent effects of the different structures on the peptide's membrane activity were also observed. The charged conformations were seen to have favorable interactions with membrane surfaces compared to a neutral Cupiennin 1a peptide. This finding agrees with the experimental solution structure of Cupiennin 1A under membrane mimicking conditions.[20] Both results highlight the importance of charged lysine residues in recognizing membrane surfaces. In terms of its cytolytic activity, however, the study was not able to observe pore formation. A future study that involves multiple Cupiennin 1a peptides on a membrane surface is recommended. Our findings here may provide insights into the structural properties of Cupiennin 1a and its antimicrobial activity toward different cell membranes.

■ METHODOLOGY

Structure Preparation. To probe the conformational space of Cupiennin 1a at pH 3 and pH 11, 100 ns all-atom HREMD simulations were performed. The starting structure for the MD simulations was obtained from the protein data bank under ID 2K38.[20] This structure corresponds to the peptide's solution structure under membrane mimicking conditions.

Cupiennin 1a is a highly cationic peptide with an estimated pI of 11.3 and a charge of +8 at neutral pH.[18] We surmise that this electrostatic property of Cupiennin 1a affects its solution structure. Hence, two solution systems were prepared for the MD simulations. One system corresponds to the positively charged peptide (pH 3) and another system is the neutral peptide (pH 11). The latter system was prepared by deprotonating the peptide's eight lysine residues. To prepare the two peptide systems for all-atom simulations, TIP3P water molecules were added until the distance between the edge of the box and the peptide is at least 10 Å.[53] The charge of the two systems was then neutralized by adding appropriate numbers of K$^+$ and Cl$^-$ ions. The physiological concentration of 0.15 M KCl was followed when adding the net-neutralizing ions. For both peptide systems, C-terminal amidation present in the original solution structure was preserved. The two systems were modeled using the CHARMM36m force field.[54]

Equilibration Step. The molecular dynamics simulations were performed using GROMACS 2019.4.[55−59] Energy minimization was performed for 5000 steps using the steepest descent method. This was followed by a 1 ns NVT equilibration set at 300 K. A time step of 2 fs was used. For both steps, the Verlet cutoff scheme was used with a cutoff distance of 1.2 nm. Long-range electrostatic interactions were calculated using the particle mesh Ewald (PME) method with a Fourier grid spacing of 0.12 nm.[60] For the NVT simulations, the solute and the solvent were coupled to a separate temperature bath using a Nose−Hoover thermostat, with a coupling time constant of 1 ps.[61] The LINCS algorithm was employed to constrain hydrogen-containing bonds.[62]

HREMD Simulations. The HREMD simulations were carried out using the REST2 method[46,47] available in GROMACS patched with plumed 2.5.6.[63] Here, the topology of the peptide was scaled by λ, a factor defined as the ratio between the lowest temperature replica, T_0, and the temperature at the ith replica, T_i. The values for λ were limited to the minimum and maximum values of $\lambda_{\min} = 0.75$ and $\lambda_{\max} = 1$, respectively. In this study, 12 replicas were simulated for 100 ns between the effective temperature range of 300 and 400 K. Calculation of the effective temperature of each replica was done using the following equation[48,49]

$$T_i = T_0 \, e^{\left[\frac{i}{n-1}\ln\left(\frac{T_{\max}}{T_0}\right)\right]}$$

The effective temperatures of the replicas were 300, 307.949, 316.109, 324.486, 333.084, 341.91, 350.97, 360.27, 369.816, 379.615, 389.674, and 400 K. Collections of frames in each replica were done every 10 ps. Exchange of replicas was attempted every 100 MD steps. The simulations were carried out in an NPT ensemble. Pressure coupling was done using the Parrinello−Rahman algorithm[64,65] with a reference pressure of 1 bar, relaxation time of 5 ps, and thermal compressibility of 4.5 x 10^{-5} bar^{-1}.

Structure−Activity Relationship. The peptide−membrane system was prepared using Membrane Builder[66] of the CHARMM-GUI webserver.[67] The peptide structures were obtained from the network analysis performed here. In total, four systems, two from each pH value, were prepared: (1) full helical and protonated peptide, (2) helix−hinge−helix and protonated peptide, (3) helix−hinge−helix and deprotonated peptide, and (4) coil-like and deprotonated peptide. The amidated C-terminal was preserved for all systems.

In four systems, the peptide was placed outside the membrane. The orientation of the peptides has their lysine residues pointing toward the phosphate heads of the lipids. A 3:1 mixture of DMPC and DMPG lipids was used to construct the membrane. About 45 DMPC and 15 DMPG lipids were placed in the upper and lower leaflets of the membrane. The Lipid17 force field was used to model the lipids. All systems have an approximate water thickness of 22.5 Å. The succeeding molecular dynamics simulations used the same parameters as the HREMD simulations.

Data Analysis. To determine conformational changes in the peptide's structure, an energy-based DSSP method was used.[68] Here, different types of secondary structures were assigned to each residue based on the interactions of internal hydrogen bonds. A hydrogen bond is defined if the energy of interaction between carbonyl oxygen atoms and amine groups is less than −0.5 kcal/mol.[68] The secondary structure of the residue is then determined by the number of residues between the internal hydrogen bond: four residues per turn for α-helices and three for 3_{10}-helices. Biophysical analyses like solvent-accessible surface area (SASA) and radius of gyration (R_g), on the other hand, were performed to visualize the possible structural changes.[69] These analyses were performed using GROMACS 2019.4.[59] Construction of the conformational space was carried out using kernel density estimation to estimate the probability density of each SASA−R_g pair obtained from all simulations.

Closely related structures were also determined through clustering analysis. In this study, the K-means clustering algorithm of cpptraj was used with an RMSD criterion of 2.5 Å.[70] A conformational cluster transition network (CCTN) was then constructed to determine possible transitions in structures.[71−73] These networks were visualized using graph-tool of the Python library.[74] Images of the structures were produced using UCSF Chimera.[75]

For the structure−activity relation studies, the minimum distance was defined as the distance between any pair of atoms between the eight lysine residues and the membrane.[76] The distance calculation was done for all the sampled conformations. The values were then binned to obtain a probability distribution of the sampled distances.

■ AUTHOR INFORMATION

Corresponding Author

Ricky B. Nellas − Institute of Chemistry, College of Science, University of the Philippines Diliman, 1101 Quezon City, Philippines; Email: rbnellas@up.edu.ph

Authors

Jokent T. Gaza − Institute of Chemistry, College of Science, University of the Philippines Diliman, 1101 Quezon City, Philippines; ◉ orcid.org/0000-0002-7836-4539

Jarold John C. Leyson − Institute of Chemistry, College of Science, University of the Philippines Diliman, 1101 Quezon City, Philippines

Gardee T. Peña − Department of Biochemistry, Faculty of Pharmacy, University of Santo Tomas, 1008 Manila, Philippines

Complete contact information is available at:
https://pubs.acs.org/10.1021/acsomega.1c03729

Author Contributions

R.B.N. conceived the project. J.T.G. performed and tested the experiments. All authors analyzed the results. All authors wrote, reviewed, and approved the final manuscript.

Notes

The authors declare no competing financial interest.

■ ABBREVIATIONS

HREMD	Hamiltonian replica-exchange molecular dynamics
AMP	antimicrobial peptide
MD	molecular dynamics
REST2	replica exchange with solute tempering 2
SASA	solvent-accessible surface area
R_g	radius of gyration

■ REFERENCES

(1) Ferreira, F. R. B.; da Silva, P. M.; Soares, T.; Machado, L. G.; de Araújo, L. C. C.; da Silva, T. G.; de Mello, G. S. V.; da Rocha Pitta, M. G.; de Melo Rego, M. J. B.; Pontual, E. V.; Zingali, R. B.; Napoleão, T. H.; Paiva, P. M. G. Evaluation of antimicrobial, cytotoxic, and hemolytic activities from venom of the spider *Lasiodora* sp. *Toxicon* **2016**, *122*, 119−126.

(2) Mourão, C. B. F.; Heghinian, M. D.; Barbosa, E. A.; Marí, F.; Bloch, C.; Restano-Cassulini, R.; Possani, L. D.; Schwartz, E. F. Characterization of a Novel Peptide Toxin from *Acanthoscurria paulensis* Spider Venom: A Distinct Cysteine Assignment to the HWTX-II Family. *Biochemistry* **2013**, *52*, 2440−2452.

(3) Sanggaard, K. W.; Bechsgaard, J. S.; Fang, X.; Duan, J.; Dyrlund, T. F.; Gupta, V.; Jiang, X.; Cheng, L.; Fan, D.; Feng, Y.; et al. Spider genomes provide insight into composition and evolution of venom and silk. *Nat. Commun.* **2014**, *5*, No. 3765.

(4) Undheim, E.; Sunagar, K.; Herzig, V.; Kely, L.; Low, D.; Jackson, T.; Jones, A.; Kurniawan, N.; King, G.; Ali, S.; Antunes, A.; Ruder, T.; Fry, B. A Proteomics and Transcriptomics Investigation of the Venom from the Barychelid Spider *Trittame loki* (Brush-Foot Trapdoor). *Toxins* **2013**, *5*, 2488−2503.

(5) Vassilevski, A. A.; Kozlov, S. A.; Grishin, E. V. Molecular diversity of spider venom. *Biochemistry* **2009**, *74*, 1505−1534.

(6) Escoubas, P. Structure and pharmacology of spider venom neurotoxins. *Biochimie* **2000**, *82*, 893−907.

(7) Wang, X.; Wang, G. Insights into Antimicrobial Peptides from Spiders and Scorpions. *Protein Pept. Lett.* **2016**, *23*, 707−721.

(8) Saez, N. J.; Herzig, V. Versatile spider venom peptides and their medical and agricultural applications. *Toxicon* **2019**, *158*, 109−126.

(9) Yan, L.; Adams, M. E. Lycotoxins, Antimicrobial Peptides from Venom of the Wolf Spider *Lycosa carolinensis*. *J. Biol. Chem.* **1998**, *273*, 2059−2066.

(10) Torres-Larios, A.; Gurrola, G. B.; Zamudio, F. Z.; Possani, L. D. Hadrurin, a new antimicrobial peptide from the venom of the scorpion *Hadrurus aztecus*. *Eur. J. Biochem.* **2000**, *267*, 5023−5031.

(11) Corzo, G.; Villegas, E.; Gómez-Lagunas, F.; Possani, L. D.; Belokoneva, O. S.; Nakajima, T. Oxyopinins, Large Amphipathic Peptides Isolated from the Venom of the Wolf Spider *Oxyopes kitabensis* with Cytolytic Properties and Positive Insecticidal Cooperativity with Spider Neurotoxins. *J. Biol. Chem.* **2002**, *277*, 23627−23637.

(12) Kuhn-Nentwig, L. Antimicrobial and cytolytic peptides of venomous arthropods. *Cell. Mol. Life Sci.* **2003**, *60*, 2651−2668.

(13) Villegas, E.; Corzo, G. Pore-Forming Peptides from Spiders. *Toxin Rev.* **2005**, *24*, 345−357.

(14) Garcia, F.; Villegas, E.; Espino-Solis, G. P.; Rodriguez, A.; Paniagua-Solis, J. F.; Sandoval-Lopez, G.; Possani, L. D.; Corzo, G. Antimicrobial peptides from arachnid venoms and their microbicidal activity in the presence of commercial antibiotics. *J. Antibiot.* **2013**, *66*, 3−10.

(15) Brown, K. L.; Hancock, R. E. Cationic host defense (antimicrobial) peptides. *Curr. Opin. Immunol.* **2006**, *18*, 24−30.

(16) Kozlov, S. A.; Vassilevski, A. A.; Feofanov, A. V.; Surovoy, A. Y.; Karpunin, D. V.; Grishin, E. V. Latarcins, Antimicrobial and Cytolytic Peptides from the Venom of the Spider *Lachesana tarabaevi* (Zodariidae) That Exemplify Biomolecular Diversity. *J. Biol. Chem.* **2006**, *281*, 20983−20992.

(17) Mattei, B.; Miranda, A.; Perez, K. R.; Riske, K. A. Structure−Activity Relationship of the Antimicrobial Peptide Gomesin: The Role of Peptide Hydrophobicity in Its Interaction with Model Membranes. *Langmuir* **2014**, *30*, 3513−3521.

(18) Kuhn-Nentwig, L.; Müller, J.; Schaller, J.; Walz, A.; Dathe, M.; Nentwig, W. Cupiennin 1, a New Family of Highly Basic Antimicrobial Peptides in the Venom of the Spider *Cupiennius salei* (Ctenidae). *J. Biol. Chem.* **2002**, *277*, 11208−11216.

(19) Kuhn-Nentwig, L.; Sheynis, T.; Kolusheva, S.; Nentwig, W.; Jelinek, R. N-terminal aromatic residues closely impact the cytolytic activity of cupiennin 1a, a major spider venom peptide. *Toxicon* **2013**, *75*, 177−186.

(20) Pukala, T.; Boland, M.; Gehman, J.; Kuhn-Nentwig, L.; Separovic, F.; Bowie, J. Solution Structure and Interaction of Cupiennin 1a, a Spider Venom Peptide, with Phospholipid Bilayers. *Biochemistry* **2007**, *46*, 3576−3585.

(21) Kuhn-Nentwig, L.; Dathe, M.; Walz, A.; Schaller, J.; Nentwig, W. Cupiennin 1d*: the cytolytic activity depends on the hydrophobic N-terminus and is modulated by the polar C-terminus. *FEBS Lett.* **2002**, *527*, 193−198.

(22) Dubovskii, P. V.; Volynsky, P. E.; Polyansky, A. A.; Chupin, V. V.; Efremov, R. G.; Arseniev, A. S. Spatial Structure and Activity Mechanism of a Novel Spider Antimicrobial Peptide. *Biochemistry* **2006**, *45*, 10759−10767.

(23) Georgescu, J.; Munhoz, V. H.; Bechinger, B. NMR Structures of the Histidine-Rich Peptide LAH4 in Micellar Environments: Membrane Insertion, pH-Dependent Mode of Antimicrobial Action, and DNA Transfection. *Biophys. J.* **2010**, *99*, 2507−2515.

(24) Pukala, T. L.; Brinkworth, C. S.; Carver, J. A.; Bowie, J. H. Investigating the Importance of the Flexible Hinge in Caerin 1.1: Solution Structures and Activity of Two Synthetically Modified Caerin Peptides. *Biochemistry* **2004**, *43*, 937−944.

(25) Joodaki, F.; Martin, L. M.; Greenfield, M. L. Computational Study of Helical and Helix-Hinge-Helix Conformations of an Anti-Microbial Peptide in Solution by Molecular Dynamics and Vibrational Analysis. *J. Phys. Chem. B* **2021**, *125*, 703−721.

(26) Sani, M.-A.; Separovic, F. Antimicrobial Peptide Structures: From Model Membranes to Live Cells. *Chem. - Eur. J.* **2018**, *24*, 286−291.

(27) Bhunia, A.; Domadia, P. N.; Torres, J.; Hallock, K. J.; Ramamoorthy, A.; Bhattacharjya, S. NMR Structure of Pardaxin, a Pore-forming Antimicrobial Peptide, in Lipopolysaccharide Micelles. *J. Biol. Chem.* **2010**, *285*, 3883−3895.

(28) Williams, J. C.; Bell, R. M. Membrane matrix disruption by melittin. *Biochim. Biophys. Acta, Biomembr.* **1972**, *288*, 255−262.

(29) Chen, J.; Guan, S.-M.; Sun, W.; Fu, H. Melittin, the Major Pain-Producing Substance of Bee Venom. *Neurosci. Bull.* **2016**, *32*, 265−272.

(30) AL-Ani, I.; Zimmermann, S.; Reichling, J.; Wink, M. Pharmacological synergism of bee venom and melittin with antibiotics and plant secondary metabolites against multi-drug resistant microbial pathogens. *Phytomedicine* **2015**, *22*, 245−255.

(31) Raghuraman, H.; Chattopadhyay, A. Melittin: a Membrane-active Peptide with Diverse Functions. *Biosci. Rep.* **2007**, *27*, 189−223.

(32) Lam, Y.; Wassall, S.; Morton, C.; Smith, R.; Separovic, F. Solid-State NMR Structure Determination of Melittin in a Lipid Environment. *Biophys. J.* **2001**, *81*, 2752−2761.

(33) Bhunia, A.; Domadia, P. N.; Bhattacharjya, S. Structural and thermodynamic analyses of the interaction between melittin and lipopolysaccharide. *Biochim. Biophys. Acta, Biomembr.* **2007**, *1768*, 3282−3291.

(34) Saravanan, R.; Bhunia, A.; Bhattacharjya, S. Micelle-bound structures and dynamics of the hinge deleted analog of melittin and its diastereomer: Implications in cell selective lysis by d-amino acid containing antimicrobial peptides. *Biochim. Biophys. Acta, Biomembr.* **2010**, *1798*, 128−139.

(35) Zasloff, M.; Martin, B.; Chen, H. C. Antimicrobial activity of synthetic magainin peptides and several analogues. *Proc. Natl. Acad. Sci. U.S.A.* **1988**, *85*, 910−913.

(36) Thennarasu, S.; Lee, D.-K.; Tan, A.; Kari, U. P.; Ramamoorthy, A. Antimicrobial activity and membrane selective interactions of a synthetic lipopeptide MSI-843. *Biochim. Biophys. Acta, Biomembr.* **2005**, *1711*, 49−58.

(37) Lamb, H. M.; Wiseman, L. R. Pexiganan Acetate. *Drugs* **1998**, *56*, 1047−1052.

(38) Maloy, W. L.; Kari, U. P. Structure-activity studies on magainins and other host defense peptides. *Biopolymers* **1995**, *37*, 105−122.

(39) Zasloff, M. Magainins, a class of antimicrobial peptides from *Xenopus* skin: isolation, characterization of two active forms, and partial cDNA sequence of a precursor. *Proc. Natl. Acad. Sci. U.S.A.* **1987**, *84*, 5449−5453.

(40) Giovannini, M. G.; Poulter, L.; Gibson, B. W.; Williams, D. H. Biosynthesis and degradation of peptides derived from *Xenopus laevis* prohormones. *Biochem. J.* **1987**, *243*, 113−120.

(41) Ramamoorthy, A.; Thennarasu, S.; Lee, D.-K.; Tan, A.; Maloy, L. Solid-State NMR Investigation of the Membrane-Disrupting Mechanism of Antimicrobial Peptides MSI-78 and MSI-594 Derived from Magainin 2 and Melittin. *Biophys. J.* **2006**, *91*, 206−216.

(42) Porcelli, F.; Buck-Koehntop, B. A.; Thennarasu, S.; Ramamoorthy, A.; Veglia, G. Structures of the Dimeric and Monomeric Variants of Magainin Antimicrobial Peptides (MSI-78 and MSI-594) in Micelles and Bilayers, Determined by NMR Spectroscopy. *Biochemistry* **2006**, *45*, 5793−5799.

(43) Bhunia, A.; Ramamoorthy, A.; Bhattacharjya, S. Helical Hairpin Structure of a Potent Antimicrobial Peptide MSI-594 in Lipopolysaccharide Micelles by NMR Spectroscopy. *Chem. - Eur. J* **2009**, *15*, 2036−2040.

(44) Domadia, P. N.; Bhunia, A.; Ramamoorthy, A.; Bhattacharjya, S. Structure, Interactions, and Antibacterial Activities of MSI-594 Derived Mutant Peptide MSI-594F5A in Lipopolysaccharide Micelles: Role of the Helical Hairpin Conformation in Outer-Membrane Permeabilization. *J. Am. Chem. Soc.* **2010**, *132*, 18417−18428.

(45) Bussi, G. Hamiltonian replica exchange in GROMACS: a flexible implementation. *Mol. Phys.* **2014**, *112*, 379−384.

(46) Wang, L.; Friesner, R. A.; Berne, B. J. Replica Exchange with Solute Scaling: A More Efficient Version of Replica Exchange with Solute Tempering (REST2). *J. Phys. Chem. B* **2011**, *115*, 9431−9438.

(47) Sugita, Y.; Okamoto, Y. Replica-exchange molecular dynamics method for protein folding. *Chem. Phys. Lett.* **1999**, *314*, 141−151.

(48) Shrestha, U. R.; Juneja, P.; Zhang, Q.; Gurumoorthy, V.; Borreguero, J. M.; Urban, V.; Cheng, X.; Pingali, S. V.; Smith, J. C.; O'Neill, H. M.; Petridis, L. Generation of the configurational ensemble of an intrinsically disordered protein from unbiased molecular dynamics simulation. *Proc. Natl. Acad. Sci. U.S.A.* **2019**, *116*, 20446−20452.

(49) Shrestha, U. R.; Smith, J. C.; Petridis, L. Full structural ensembles of intrinsically disordered proteins from unbiased molecular dynamics simulations. *Commun. Biol.* **2021**, *4*, No. 243.

(50) Kuhn-Nentwig, L.; Willems, J.; Seebeck, T.; Shalaby, T.; Kaiser, M.; Nentwig, W. Cupiennin 1a exhibits a remarkably broad, non-stereospecific cytolytic activity on bacteria, protozoan parasites, insects, and human cancer cells. *Amino Acids* **2011**, *40*, 69−76.

(51) Wang, Y.; Zhao, T.; Wei, D.; Strandberg, E.; Ulrich, A. S.; Ulmschneider, J. P. How reliable are molecular dynamics simulations of membrane active antimicrobial peptides? *Biochim. Biophys. Acta, Biomembr.* **2014**, *1838*, 2280−2288.

(52) Ulmschneider, J. P.; Smith, J. C.; Ulmschneider, M. B.; Ulrich, A. S.; Strandberg, E. Reorientation and Dimerization of the Membrane-Bound Antimicrobial Peptide PGLa from Microsecond All-Atom MD Simulations. *Biophys. J.* **2012**, *103*, 472−482.

(53) Jorgensen, W. L.; Chandrasekhar, J.; Madura, J. D.; Impey, R. W.; Klein, M. L. Comparison of simple potential functions for simulating liquid water. *J. Chem. Phys.* **1983**, *79*, 926−935.

(54) Huang, J.; Rauscher, S.; Nawrocki, G.; Ran, T.; Feig, M.; de Groot, B. L.; Grubmüller, H.; MacKerell, A. D. CHARMM36m: an improved force field for folded and intrinsically disordered proteins. *Nat. Methods* **2017**, *14*, 71−73.

(55) Berendsen, H.; van der Spoel, D.; van Drunen, R. GROMACS: A message-passing parallel molecular dynamics implementation. *Comput. Phys. Commun.* **1995**, *91*, 43−56.

(56) Lindahl, E.; Hess, B.; van der Spoel, D. GROMACS 3.0: a package for molecular simulation and trajectory analysis. *J. Mol. Model.* **2001**, *7*, 306−317.

(57) Van Der Spoel, D.; Lindahl, E.; Hess, B.; Groenhof, G.; Mark, A. E.; Berendsen, H. J. C. GROMACS: Fast, flexible, and free. *J. Comput. Chem.* **2005**, *26*, 1701−1718.

(58) Abraham, M. J.; Murtola, T.; Schulz, R.; Páll, S.; Smith, J. C.; Hess, B.; Lindahl, E. GROMACS: High performance molecular simulations through multi-level parallelism from laptops to super-computers. *SoftwareX* **2015**, *1−2*, 19−25.

(59) Lindahl, E.; Abraham, M. J.; Hess, B.; van der Spoel, D. *GROMACS 2019.4 Source code.* https://zenodo.org/record/3460414, 2019.

(60) Darden, T.; York, D.; Pedersen, L. Particle mesh Ewald: An N·log(N) method for Ewald sums in large systems. *J. Chem. Phys.* **1993**, *98*, 10089−10092.

(61) Evans, D. J.; Holian, B. L. The Nose−Hoover thermostat. *J. Chem. Phys.* **1985**, *83*, 4069−4074.

(62) Hess, B.; Bekker, H.; Berendsen, H. J. C.; Fraaije, J. G. E. M. LINCS: A linear constraint solver for molecular simulations. *J. Comput. Chem.* **1997**, *18*, 1463−1472.

(63) Bonomi, M.; Branduardi, D.; Bussi, G.; Camilloni, C.; Provasi, D.; Raiteri, P.; Donadio, D.; Marinelli, F.; Pietrucci, F.; Broglia, R. A.; Parrinello, M. PLUMED: A portable plugin for free-energy calculations with molecular dynamics. *Comput. Phys. Commun.* **2009**, *180*, 1961−1972.

(64) Parrinello, M.; Rahman, A. Polymorphic transitions in single crystals: A new molecular dynamics method. *J. Appl. Phys.* **1981**, *52*, 7182−7190.

(65) Nosé, S.; Klein, M. Constant pressure molecular dynamics for molecular systems. *Mol. Phys.* **1983**, *50*, 1055−1076.

(66) Wu, E. L.; Cheng, X.; Jo, S.; Rui, H.; Song, K. C.; Dávila-Contreras, E. M.; Qi, Y.; Lee, J.; Monje-Galvan, V.; Venable, R. M.; Klauda, J. B.; Im, W. CHARMM-GUI Membrane Builder toward realistic biological membrane simulations. *J. Comput. Chem.* **2014**, *35*, 1997−2004.

(67) Jo, S.; Kim, T.; Iyer, V. G.; Im, W. CHARMM-GUI: A web-based graphical user interface for CHARMM. *J. Comput. Chem.* **2008**, *29*, 1859−1865.

(68) Kabsch, W.; Sander, C. Dictionary of protein secondary structure: Pattern recognition of hydrogen-bonded and geometrical features. *Biopolymers* **1983**, *22*, 2577−2637.

(69) Eisenhaber, F.; Lijnzaad, P.; Argos, P.; Sander, C.; Scharf, M. The double cubic lattice method: Efficient approaches to numerical integration of surface area and volume and to dot surface contouring of molecular assemblies. *J. Comput. Chem.* **1995**, *16*, 273−284.

(70) Roe, D. R.; Cheatham, T. E. PTRAJ and CPPTRAJ: Software for Processing and Analysis of Molecular Dynamics Trajectory Data. *J. Chem. Theory Comput.* **2013**, *9*, 3084−3095.

(71) Noé, F.; Fischer, S. Transition networks for modeling the kinetics of conformational change in macromolecules. *Curr. Opin. Struct. Biol.* **2008**, *18*, 154−162.

(72) Noé, F.; Horenko, I.; Schütte, C.; Smith, J. C. Hierarchical analysis of conformational dynamics in biomolecules: Transition networks of metastable states. *J. Chem. Phys.* **2007**, *126*, No. 155102.

(73) Braza, M. K. E.; Gazmen, J. D. N.; Yu, E. T.; Nellas, R. B. Ligand-Induced Conformational Dynamics of A Tyramine Receptor from Sitophilus oryzae. *Sci. Rep.* **2019**, No. 16275.

(74) Peixoto, T. P. *The graph-tool python library. figshare*, 2014.

(75) Pettersen, E. F.; Goddard, T. D.; Huang, C. C.; Couch, G. S.; Greenblatt, D. M.; Meng, E. C.; Ferrin, T. E. UCSF Chimera − A visualization system for exploratory research and analysis. *J. Comput. Chem.* **2004**, *25*, 1605−1612.

(76) Shepherd, C. M.; Schaus, K. A.; Vogel, H. J.; Juffer, A. H. Molecular Dynamics Study of Peptide-Bilayer Adsorption. *Biophys. J.* **2001**, *80*, 579−596.